# IV-J Development of Pulsed Field Gradient NMR Spectroscopy

Pulsed field gradient spin echo (PGSE) nuclear magnetic resonance (NMR) is a powerful method for the study of dynamics in condensed matter since it probes translational motion of molecules selectively, without being affected by vibrational or rotational motions. Due to this advantage it has been widely applied to the dynamics of molecules in liquids. However, applications of this technique to strongly dipole-coupled spin systems with short $T_2$ or to the study of slow and anisotropic self-diffusion are still challenging works because combined techniques of line-narrowing, pulsing of sharp and intense field gradients, and two-dimensional field-gradient generation are necessary.

In the present study we applied the technique to the study of anisotropic self-diffusion in liquid crystals, with the use of the laboratory-made spectrometer equipped with a rotatable quadrupole gradient coil.

## IV-J-1 Self-diffusion Coefficients of a Reentrant Liquid Crystal CBOBP

**OISHI, Osamu; MIYAJIMA, Seiichi**

Self-diffusion coefficient tensors of a reentrant liquid crystal CBOBP were measured in the high and low temperature $S_A$ phases. In the high temperature $S_A$ phase, the diffusion coefficient component $D_{//}$ is larger than $D_\perp$. The two activation energies are similar. This property resembles that of the nematic phase, and indicates that the layer structure of the high temperature $S_A$ phase is disordered remarkably. In the low temperature $S_A$ phase, absolute values of the self-diffusion coefficient components, $D_{//}$ and $D_\perp$, are close to each other, in contrast with the diffusion coefficient components in the high temperature $S_A$ phase. The activation energy for $D_{//}$ is much higher than that for $D_\perp$. This suggests a firm layer structure. It is also interesting to note that the activation energies for $D_\perp$ are similar in the high and low temperature $S_A$ phases, and the values of $D_\perp$ are found on one straight line through both phases. Taking these in mind there seems to be no change in molecular interaction and molecular arrangement in the two $S_A$ phases, as far as the perpendicular components concern. The change in molecular interaction and structure seemed to have occurred in the parallel components.

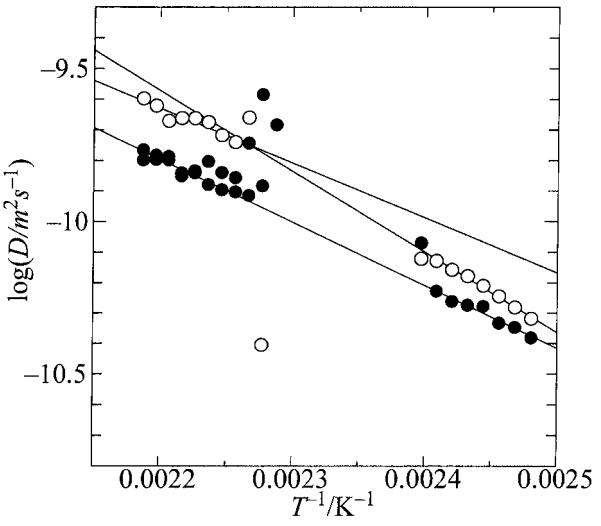


**Figure 1.** Anisotropic self-diffusion coefficients of CBOBP in smectic A phases (○ $D_{//}$, ● $D_\perp$).

## IV-J-2 Self-diffusion Coefficients of OBBC and OBBF

**OISHI, Osamu; MIYAJIMA, Seiichi**

OBBC is a reentrant liquid crystal. OBBF is a derivative of OBBC, where the terminal cyano group in OBBC is replaced by fluorine, and shows no reentrant phases. In the $S_A$ phase of OBBC between the two nematic phases, the self-diffusion coefficient component $D_{//}$ is larger than $D_\perp$. The activation energies for both $D_{//}$ and $D_\perp$ are low, and similar in magnitudes.

OBBF exhibits a remarkable feature. $D_{//}$ is higher than $D_\perp$, and the relative magnitudes of $D_{//}$ and $D_\perp$ reverses with the change of temperature. The self-diffusion property in the $S_A$ phase of OBBC resembles that in the high temperature phase of CBOBP, and the self-diffusion property of OBBF is close to that of the low temperature phase of CBOBP.

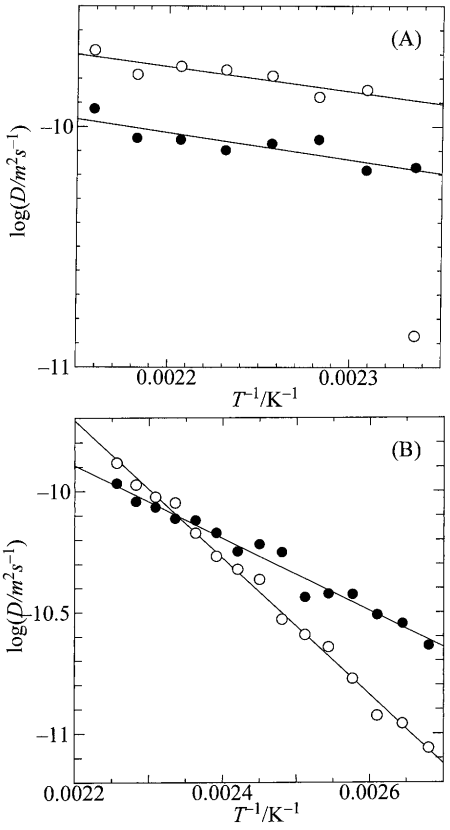


**Figure 1.** Anisotropic self-diffusion coefficients of OBBC(A) and OBBF(B) in smectic A phases (○ $D_{//}$, ● $D_\perp$)

### IV-J-3 Self-Diffusion Coefficients of an Anti-Ferroelectric Liquid Crystal MHPOBC

**OISHI, Osamu; MIYAJIMA, Seiichi**

The anti-ferroelectric liquid crystal MHPOBC shows various phase structures with temperature change. It was found that the activation energy for $D_{//}$ was much higher than that for $D_{\perp}$ even in the para-electric $S_A$ phase, and so the formation of a firm layer structure was indicated. Smaller values of $D_{//}$ indicate that diffusion across the layers is difficult.

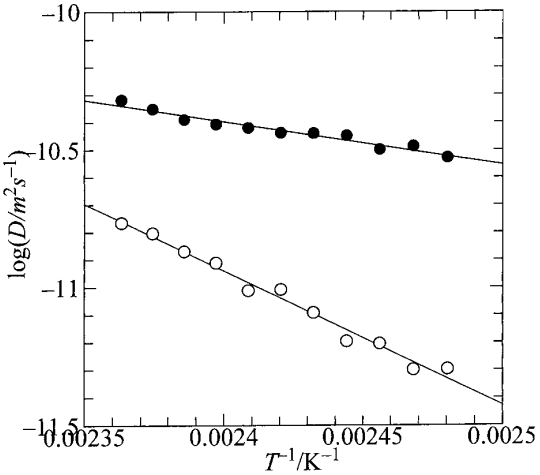


**Figure 1.** Anisotropic self-diffusion coefficients of MHPOBC in smectic A phase (○ $D_{//}$, ● $D_{\perp}$).

### IV-J-4 Self-diffusion Coefficients of a Hexatic Liquid Crystal PHOAB

**OISHI, Osamu; MIYAJIMA, Seiichi**

PHOAB exhibits a phase transition sequence, $S_A$ — hexatic smectic B— crystalline smectic B, on lowering the temperature. In the $S_A$ phase, the activation energy for $D_{//}$ is much higher than that for $D_{\perp}$. This fact shows that a firm layer structure is formed. At the phase transition from $S_A$ to hexatic B, the self-diffusion coefficients become small to a level where even the perpendicular component was immeasurable. The diffusion properties of PHOAB and OBBF are similar: $D_{//}$ and $D_{\perp}$ have similar values at high temperature, but $D_{//}$ becomes smaller in comparison with $D_{\perp}$ at low temperature.

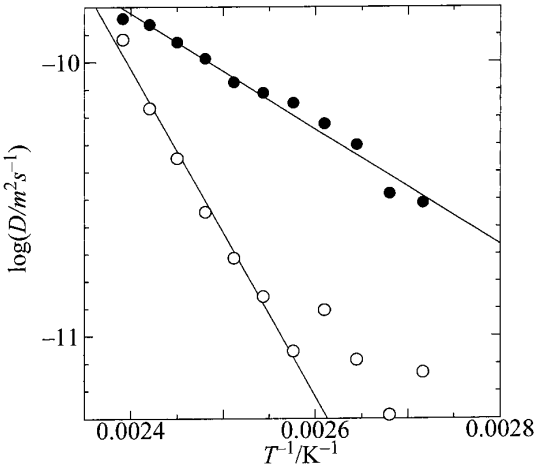


**Figure 1.** Anisotropic self-diffusion coefficients of PHOAB in smectic A phase (○ $D_{//}$, ● $D_{\perp}$)

### IV-J-5 Calculation of Dipole Moments by MOPAC7

**OISHI, Osamu; MIYAJIMA, Seiichi**

Dipole moments were calculated with the MOPAC7 program. The calculated values are 5.8 (OBBC), 4.2 (OBBF), 6.4 (CBOBP), 2.5 (MHPOBC), and 4.3 (PHOAB) Debyes. The reentrant nematic liquid crystals, OBBC and CBOBP, have larger dipole moments.

### IV-J-6 Measurement of Anisotropic Self-Diffusion Coefficient Tensors by PGSE-NMR

**MIYAJIMA, Seiichi; OISHI, Osamu**

[*DIM Newsletter* **12**, 16 (1998)]

A review account is given for the pulsed field gradient spin echo (PGSE) NMR technique, which has been applied to the determination of anisotropic self-diffusion coefficient tensors. Principles and methods are explained, and their applications to the translational dynamics of liquid crystals is presented.

## IV-K Phase Transitions and Dynamical Ordering in Liquid Crystals

Extensive high resolution NMR studies were conducted to reveal the dynamics and the microscopic origin of antiferroelectricity in liquid crystals.

### IV-K-1 A Bent and Asymmetrically Hindered Chiral Alkyl Chain of an Antiferroelectric Liquid Crystal as Observed by $^2$H NMR

**YOSHIDA, Shohei[1]; JIN, Bo[1]; TOKUMARU, Koh[1]; TAKANISHI, Yoichi[1]; ISHIKAWA, Ken[1]; TAKEZOE, Hideo[1]; FUKUDA, Atsuo[2]; KUSUMOTO, Tetsuo[3]; NAKAI, Toshihito[4]; MIYAJIMA, Seiichi**
*([1]Tokyo Inst. Tech.; [2]Shinshu Univ.; [3]Sagami Cent. Res. Cent.; [4]Tokyo Univ. Agric. Tech.)*

[*J. Phys. Soc. Jpn.* **68**, 46 (1999)]

The structure and dynamics of the alkyl chains are

investigated by $^2$H-NMR for specifically deuterated samples of an antiferroelectric liquid crystal MHPOBC. The $^2$H-NMR spectrum for the chiral alkyl chain exhibits very small quadrupolar splittings, and the methylenes close to the chiral center give double splittings, which are ascribable to two different quadrupolar splittings for each methylene unit. The unusual nature of the chiral chain is revealed; the chain is bent from the molecular long axis, and its motion is asymmetrically hindered.

### IV-K-2 Experimental Spectroscopy of Liquid Crystals, No. 4-6. NMR Spectroscopy, Pt. 1-3

**MIYAJIMA, Seiichi; NAKAI, Toshihito[1]**
*([1]Tokyo Univ. Agric. Tech.)*

[*EKISHO* **3**, 43, 124 and 205 (1999)]

NMR study of liquid crystals is outlined in a series of lectures, with special emphasis on its methodological aspects. Pt. 1 describes the theoretical framework for the spectral analysis, in connection with the orientational order parameters. Pt. 2 deals with various aspects of experimental $^{13}$C NMR spectroscopy. Determination of the order parameters by the alignment-induced shifts, and determination of the nuclear shielding tensor elements by two-dimensional (2-D) site-separated spinning sideband spectroscopy are described. Use of partially averaged $^{13}$C-$^1$H dipolar interactions is shown in the experiments of transient oscillation in cross-polarized magnetization, and 2-D dipolar separated-local field spectroscopy. Analysis of molecular rotational motion by relaxation measurements is also shown. Pt. 3 describes how $^2$H NMR is applied to solve various important problems of liquid crystals, such as determination of segmental order parameters, detection of asymmetrical hindrance in rotational motions, and detection of the phase biaxiality. Finally the pulsed field gradient spin-echo NMR technique is explained, and it is shown how the translational self-diffusion coefficient tensor elements are determined.

# IV-L Electronic Properties of Alkali-Hydrogen-Carbon Systems

In alkali-hydrogen-carbon ternary systems, hydrogen or alkali metal elements exhibit a variety of electronic states when doped or intercalated in the host crystal lattice. An interesting feature is how the hydrogen 1s state contribute to the bulk electronic properties. Structural and electronic properties were studied for stage-6 sodium-hydrogen-graphite ternary compound by means of solid state NMR. New alkali-hydrogen-$C_{70}$ compounds were synthesized by detecting and controlling the reaction of alkali hydrides with $C_{70}$ crystal with *in-situ* $^1$H NMR measurements and characterized the structures and the magnetic properties by powder X-ray diffraction, ESR and magnetic susceptibility measurements. New alkali-hydrogen-single-walled carbon nanotube aggregates were synthesized and characterized by solid state NMR.

### IV-L-1 NMR Study of Stage-6 Sodium-Hydrogen-Graphite Intercalation Compound

**OGATA, Hironori; MIYAJIMA, Seiichi; ENOKI, Toshiaki[1]; ANTOINE, Laurence[2]; GUERARD, Daniel[2]**
*([1]Tokyo Inst. Tech.; [2]Univ. Nancy I )*

$^{23}$Na, $^1$H and $^{13}$C NMR have been carried out for stage-6 sodium-hydrogen-graphite intercalation compound (NaH-GIC). Figure 1 shows the $^1$H decoupled $^{13}$C NMR spectra in stage-6 NaH-GIC with the external field ($B_0$) perpendicular (a) and parallel (b) to the *c*-axis. The lines 1α and 1β correspond to the inequivalent two carbon atoms on the bounding layer (layer 1), and 2α, 2β and 3α, 3β correspond to those on middle and interior layer (layer 2 and 3), respectively. From the anisotropic values of $^{13}$C NMR shifts, the charge transfer rates per one carbon atom were estimated to be 0.028, 0.005 and 0.001 for layer 1, 2 and 3, repectively. Figure 2 shows the angluar dependence of the $^1$H NMR second moment $<\Delta\nu^2>$ measured at room temperature. $<\Delta\nu^2>$ has has its minimum at around 40°, which suggests that hydrogen forms two-dimensional lattice in the intercalate. However, the values of $<\Delta\nu^2>$ obtained were much larger than those expected from the model calculation. This fact suggests the existence of paramagnetic defects in the intercalate, which was reported for higher stage NaH-GIC sample by ESR measurement. The angular dependence of $^{23}$Na NMR spectrum showed the existence of two $Na^+$ sites with different electric field gradient tensors.

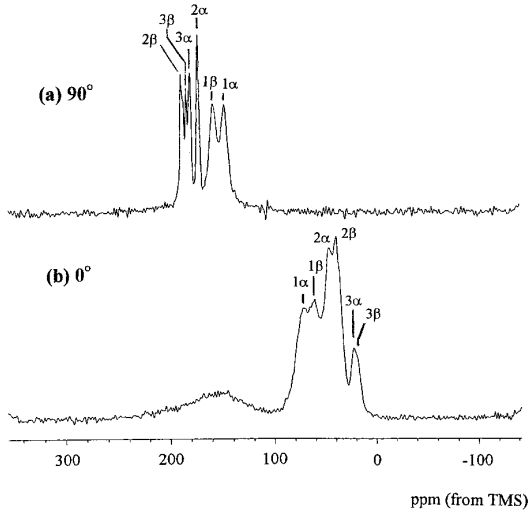


**Figure 1.** $^1$H decoupled $^{13}$C NMR spectra in stage-6 NaH-GIC with the external field ($B_0$) perpendicular (a) and parallel (b) to the *c*-axis.

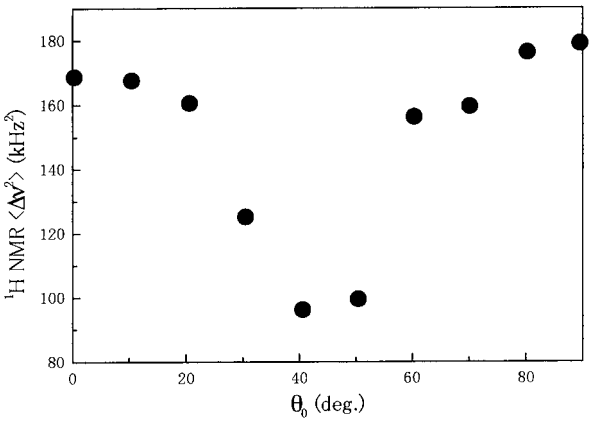


**Figure 2.** Angular dependence of the $^1$H NMR second moment in stage-6 NaH-GIC measured at room temperature.

## IV-L-2 *In-situ* NMR Study of the Reaction Process in Alkali-Hydrogen-Fullerene Systems

**OGATA, Hironori**

In the previous work, we have reported the attempts at detecting and controlling the reaction of potassium hydride (KH) or sodium hydride (NaH) with $C_{60}$ crystal with *in-situ* $^1$H NMR measurements. We also conducted with those of NaH or KH with $C_{70}$ crystal. Figure 1 shows the time dependence of $^1$H NMR spectra for a mixture of stoichiometric amounts (3:1) of NaH and $C_{70}$ reacted at 503 K (a) and of KH and $C_{70}$ at 450 K (b), respectively. After several minutes' reaction, a signal at about –4 ppm appeared, which may be ascribable to decomposition of KH or NaH. Just after the intensity of this peak became maximum, the sample was cooled rapidly to 150 K to stop the reaction. After cooling, the hydrogen peak disappeared for NaH-$C_{70}$ sample but stablized as hydrogen anion for KH-$C_{70}$ sample. This peak intensity, however, gradually decreased after the sample was heated up to room temperature and disappeared within 24 hrs. Powder X-ray diffraction profile of the KH-$C_{70}$ sample just after the reation showed that these crystals form fcc structure with lattice constant $a$ = 15.04 Å at room temperature. This value is larger than that of fcc $K_3C_{70}$ ($a$ = 14.96 Å at room temperature). These facts suggest that hydrogen anion is occupied in the interstitial site of the $K_3C_{70}$ crystal just after the reaction. Figure 2 shows the temperature dependence of the magnetic susceptibilty of $K_3H_xC_{70}$ just after the reaction. A small but distinct anomaly, which was not reported for $K_3C_{70}$ was observed at 120 K. This anomaly was also observed in the temperature dependence of ESR peak-to-peak linewidth ($\Delta H_{p\text{-}p}$) for $K_3H_xC_{70}$ (Figure 3). The value of Pauli-paramagnetic susceptibility was evaluated to be about $7 \times 10^{-4}$ emu/mole from ESR and magnetic susceptibility measurements.

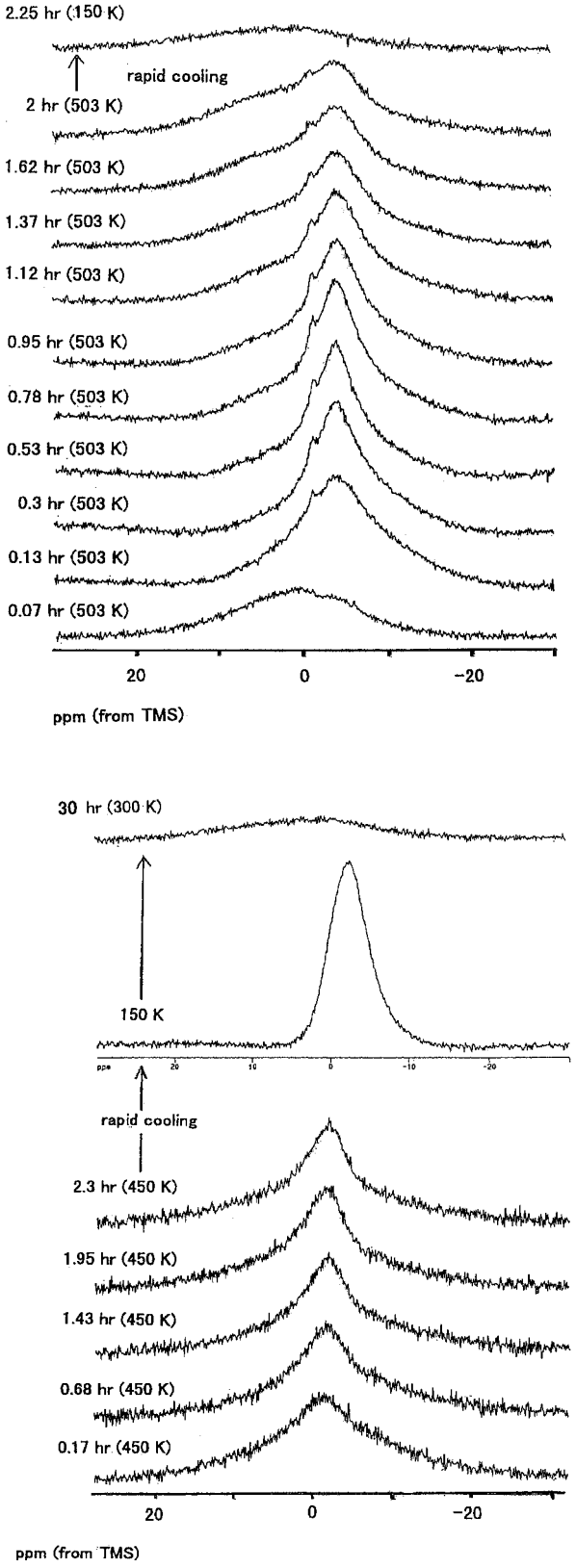


**Figure 1.** Time dependence of *in-situ* $^1$H NMR spectra for the mixture of (a) NaH and $C_{70}$ and of (b) KH and $C_{70}$.

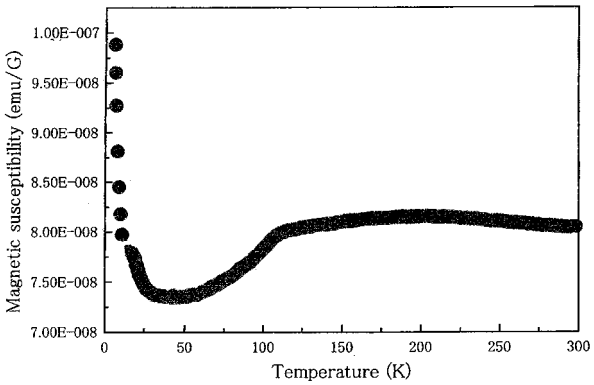


**Figure 2.** Temperature dependence of static magnetic susceptibilty of $K_3H_xC_{70}$ just after the reaction.

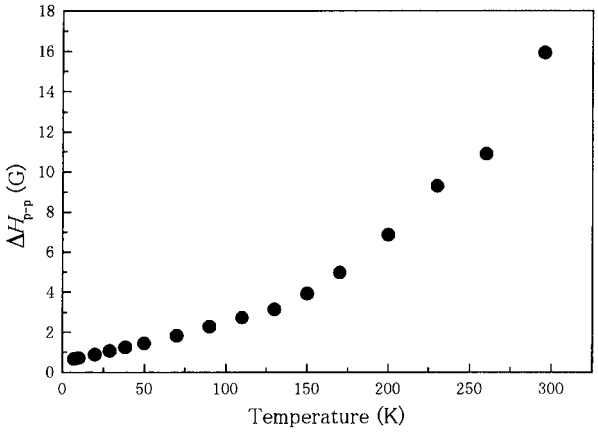


**Figure 3.** Temperature dependence of ESR peak-to-peak linewidth for $K_3H_yC_{70}$ just after the reaction.

### IV-L-3 Synthesis and NMR study of Alkali-Hydrogen-Single-Walled Carbon Nanotubes

**OGATA, Hironori; BANDOW, Syunji[1]; KUNO, Syougo[2]; SAITO, Yahachi[2]**
*([1]ICORP-JST; [2]Mie Univ.)*

Potassum-hydrogen-single-walled carbon nanotubes (K-H-SWNTs) aggregates were synthesized first and their states of hydrogen were studied by solid state $^1$H NMR. Rh-Pt mixed catalysts and hydrogen peroxide were used to produce SWNTs and remove amorphous carbon particles in the raw soot. Two kinds of SWNTs were prepared as starting sample, one was the SWNTs with caps and the other was those without caps obtained by a heating treatment in dried air. K-H-SWNTs samples were synthesized by both (a) the direct reaction of potassium hydride (KH) and SWNTs and (b) the absoption of $H_2$ gas on K-doped SWNTs. $^1$H NMR measurements proved that a singlet $^1$H spectrum with the value of the second moment of about 40 kHz$^2$ at –10 ppm (from TMS) was observed only by using uncaped SWNTs as starting samples, independently of the way of synthesis. This fact suggests that hydrogen anion is condensed inside SWNTs for K-H-SWNTs (uncaped) system.

# IV-M Strutural and Electronic Properties of New Carbon Materials

Electronic properties and the function of micropores were studied for new carbon materials in this project. $^{13}$C NMR were performed first for single-walled carbon nanotubes (SWNTs) to investigate the electronic structure in the magnetic field. The behavior of water molecules absorbed in activated carbon fiber (ACF) was studied by solid state $^1$H NMR.

### IV-M-1 $^{13}$C NMR Study of Single-Walled Carbon Nanotubes

**OGATA, Hironori; BANDOW, Syunji[1]; KUNO, Syougo[2]; SAITO, Yahachi[2]**
*([1]ICORP-JST; [2]Mie Univ.)*

$^{13}$C NMR experiments have been carried out for single-walled carbon nanotubes (SWNTs), which were produced by using non-ferromagnetic Rh-Pt mixed catalysts. Hydrogen peroxide was used to remove amorphous carbon particles in the raw soot almost perfectly. Figure 1 shows the $^{13}$C NMR spectrum at 298 K. From the line shape analysis of the $^{13}$C spectrum, the shift tensor was evaluated to be ($\delta_{11}$, $\delta_{22}$, $\delta_{33}$) = (192, 186, 132) ppm. Small anisotropic value ($\Delta\delta$ = –57 ppm) compared with that reported for MWNTs[1)] suggests that this SWNTs sample contains metallic tubes with larger electronic density of states at the Fermi level than that of MWNTs sample. Furthermore, the intensity of $^{13}$C signal was found to be weak for the amount of the sample, suggesting that the $^{13}$C signal observed was only from metallic tubes. The $^{13}$C NMR signal of semi-conducting tubes was broadened and could not be observed virtually due to the large anisotropy of diamagnetic susceptibility, which is theoretically predicted.[2)]

To obtain more detailed information about the electronic state of SWNTs, we performed $^{13}$C spin lattice relaxation time ($T_1$) measurement at 100.1 MHz (9.4 T). Figure 2 shows the temperature dependence of spin-lattice relaxation time at 9.4 T. It is found that SWNTs follows a Korringa-like behavior ($T_1 \times T$ = 940 ± 60 (sec.K)) in the temperature region between 4.2 K and 100 K, which is different largely with that of graphite sample.[3)] This fact suggests that metallic tubes exist at the magnetic field of 9.4 T.

**References**

1) Y. Maniwa *et al.*, *Proc. XII Int. Winterschool* (Kirchberg, Austria) 87 (1998).
2) Ajiki and Ando, *J. Phys. Soc. Jpn.* **62**, 2470 (1993).
3) K. Kume *et al.*, *Synth. Met.* **12**, 307 (1985).

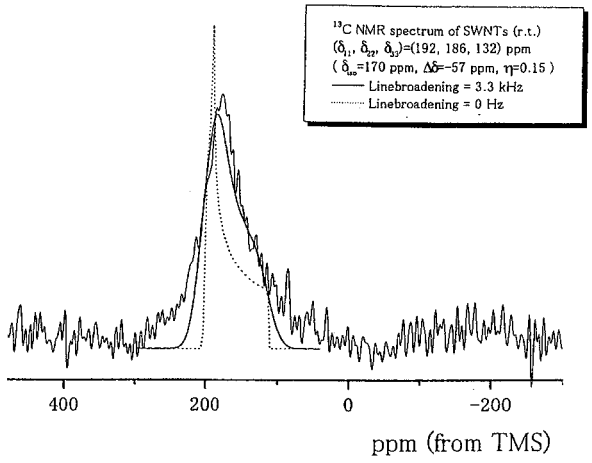


**Figure 1.** $^{13}$C NMR spectrum of SWNTs at 298 K.

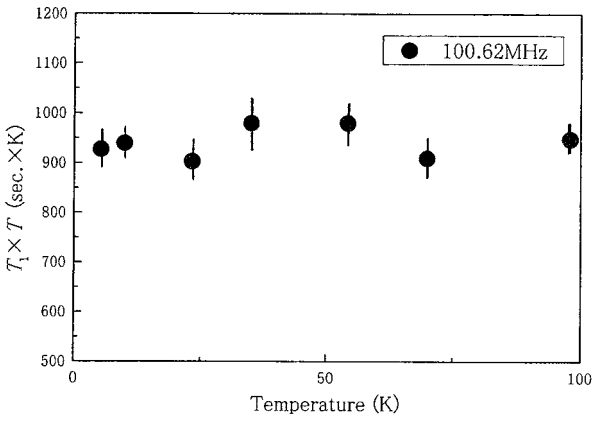


**Figure 2.** Temperature ependence of $^{13}$C $T_1 \times T$ of SWNTs at 9.4 T.

## IV-M-2 Dynamics of Water Molecules Confined in Activated Carbon Fiber

**OGATA, Hironori; MIYAJIMA, Seiichi; YOSHIKAWA, Yuuhi[1]; SATO, Hirohiko[1]; ENOKI, Toshiaki[1]**
*([1]Tokyo Inst. Tech.)*

Water molecules adsorbed in microporous carbon materials are expected to show distinctive characteristics different from those in the bulk state. For example, since micrographite surfaces in carbon materials are hydrophobic, if water is adsorbed, its structure is essentially affected by either the confinement effect or the hydrophobic effect originating in the interaction with carbon surfaces. $^1$H NMR measurements were conducted for water molecules adsorbed in activated carbon fiber (ACF). At room temperature the lineshape of the $^1$H NMR spectrum for this system consists of two peaks at –0.4 ppm and –3.9 ppm (from TMS) with inhomogeneous broadenings, which are considered to be attribute to the difference of the adsorption sites of water molecules. The temperature dependence of the value of the $^1$H NMR second moment ($<\Delta\nu^2>$) is shown in Figure 1. With decreasing temperature, $<\Delta\nu^2>$ increased drastically at about 190 K and a plateau of 55 kHz$^2$ was observed below 160 K, which was much smaller than that of bulk ice (about 345 kHz$^2$ at 200 K). The peak position of the $^1$H NMR spectrum at 160 K was +10 ppm. These facts suggests that water molecules confined in ACF micropores freeze and form a hydrogen-bonded network at 160 K and that strong interaction between water molecules and ACF micropores surface hinders the the growth of three-dimensional hydrogen-bonded network. Figure 2 shows the temperaure dependence of $^1$H NMR spin-lattice relaxation time ($T_1$) for this system. The distinct minimum of the $T_1$ at 225 K was observed, which is thought to be associated with the self-diffusion of the water molecules. The activation energy ($E_a$) and the correlation time ($\tau_c$) at 298 K were evaluated to be 2.7 kcal/mole, and $5.5 \times 10^{-11}$ sec., respectively. The value of $E_a$ obtained is almost same as that of the self-diffusion for bulk water (4 kcal/mole), however, the value of $\tau_c$ is much larger than that of bulk water ($2.5 \times 10^{-12}$ sec. at 298 K) due to the confinement effect.

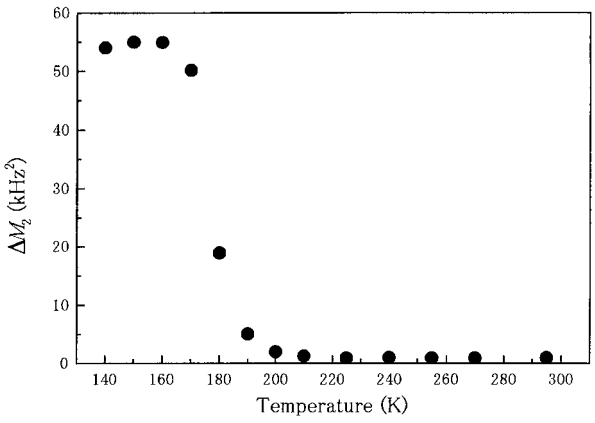


**Figure 1.** Temperature dependence of $^1$H NMR second moment for water adsorbed activated carbon fiber.

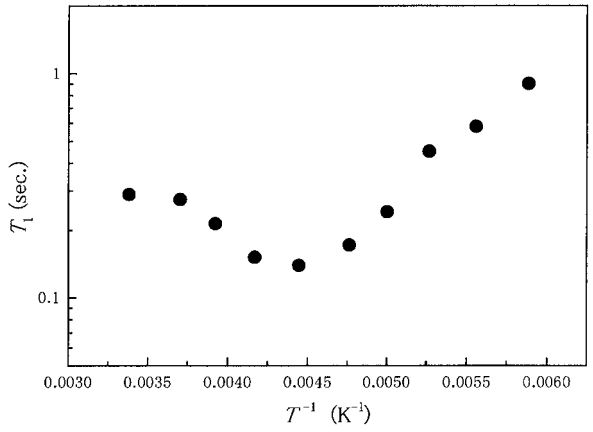


**Figure 2.** Temperature dependence of $^1$H NMR spin-lattice relaxaton time for water adsorbed activated carbon fiber.

# IV-N Structural and Electronic Properties of Fullerene-Based Compounds

Structural and electronic properties were studied for several types of fullerene-based compounds in this project. Electronic and magnetic properties of $Na_x(THF)_yC_{60}$ single crystals were studied by magnetic susceptibility, ESR and Raman scattering measurements. $^1H$, $^{23}Na$ and $^{13}C$ NMR studies were conduted for $Na_x(THF)_yC_{60}$ single crystals to reveal the miroscopic origins of the phase tranitions and the structural and electronic states at low temperature. Attempts at doping Ce into $C_{60}$ crystal were conducted and structural and magnetic properties of the products were investigated. Raman scatterings and X-ray powder diffractions for a pressure induced superconductor $Cs_3C_{60}$ were studied under some pressures.

## IV-N-1 Electronic Properties of Alkali-THF-$C_{60}$ Single Crystals

**OGATA, Hironori; KOBAYASHI, Hayao; YAKUSHI, Kyuya; MORIYAMA, Hiroshi[1]**
*([1]Toho Univ.)*

The electronic and magnetic properties of $Na_x(THF)_yC_{60}$ single crystals were studied by means of ESR, magnetic susceptibility, and Raman scattering measurements. Figure 1 shows the temperature dependence of ESR peak-to-peak linewidth ($\Delta H_{p\text{-}p}$) for $Na_x(THF)_yC_{60}$. The value of $\Delta H_{p\text{-}p}$ decreases monotonically with decreasing temperature in the temperature region between 300 K and 10 K with sudden drop at 180 K. This drop is attributed to be metal-metal phase trnasition previously reported for this compound.[1)] Pauli susceptibility at room temperature was evaluated to be $\chi_P = 3.6 \times 10^{-4}$ (emu/mol) from ESR measurement. Figure 2 shows the temperature dependence of magnetic susceptibility for $Na_x(THF)_yC_{60}$. Two small reduction in the magnetic susceptibility were observed below 180 K and 50 K, the former is attributed to be metal-metal phase trnasition above-mentioned. The temperature dependence of the peak position of the $A_g(2)$ mode of $C_{60}$ in $Na_x(THF)_yC_{60}$ revealed that the molecular valence of $C_{60}$ was –1 in the temperature region between 298 K and 4.2 K. In conclusion, it was found that $Na_x(THF)_yC_{60}$ is a metal down to 4.2 K, which is composed of $C_{60}^{1-}$ anions.

**Reference**

1) H. Kobayashi *et al.*, *J. Am. Chem. Soc.* **116**, 3153 (1994).

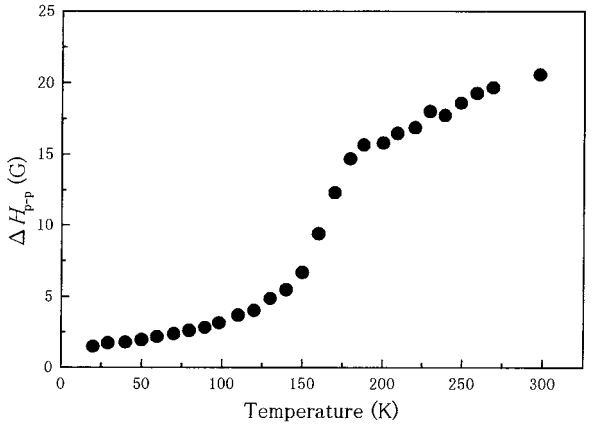


**Figure 1.** Temperature dependence of ESR peak-to-peak linewidth ($\Delta H_{p\text{-}p}$) for $Na_x(THF)_yC_{60}$ single crystals.

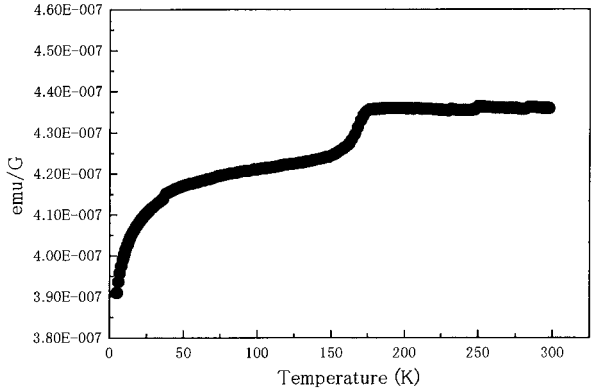


**Figure 2.** Temperature dependence of magnetic susceptibility for $Na_x(THF)_yC_{60}$ single crystals.

## IV-N-2 NMR Study of Sodium-THF-$C_{60}$ Single Crystals

**OGATA, Hironori; KOBAYASHI, Hayao; MORIYAMA, Hiroshi[1]**
*([1]Toho Univ.)*

$^1H$, $^{23}Na$ and $^{13}C$ NMR measurements were performed for $Na(THF)_yC_{60}$ single crystals to elucidate the microscopic origins of the phase transitions at 180 K and 50 K and the electronic state at low temperature. Figure 1 shows the temperature dependence of $^{23}Na$ NMR spectrum for $Na(THF)_yC_{60}$. A singlet spectrum appearing at –7 ppm (from 1.0 M NaCl aqu.sol.) at 297 K suggests that more than four THF molecules are coordinated around the $Na^+$ ions. The $^{23}Na$ linewidth does not undergo the remarkable change at 180 K, while the line brodening is observed below 50 K. Figure 2 shows the temperature dependence of $^1H$ NMR spectrum for $Na(THF)_yC_{60}$. The $^1H$ linewidth changed clearly at 180 K. At 160 K, the linewidth of $^1H$ NMR spectrum ($\Delta H_{1/2}$) is evaluated to be about 8 G, which is smaller than that of motionless THF molecules (~15 G). No significant change was observed at 180 K in the temperature dependence of the line shape of $^{13}C$ NMR spectrum. These facts are explicalble by assuming that the librational motion around the axis connecting between sodium cation and the oxygen of the THF molecule freezes below 180 K and the hydrogen of the $-CH_2-$ group becomes motionless below 50 K in the time scale of NMR. The temperature dependence of the $^{13}C$ nuclear spin-lattice relaxaton rate, $T_1^{-1}$, exhibited Korringa-like behavior ($T_1 \times T = 550$ (sec × K)) in the temperature region between 50 K and 6 K. This facts suggests that $Na(THF)C_{60}$ is metallic down to 6 K. The

electronic density of states at Fermi level of this compound was evaluated to be about 30% of that of $K_3C_{60}$ superconductor, provided that these electronic correlation effects are equal.

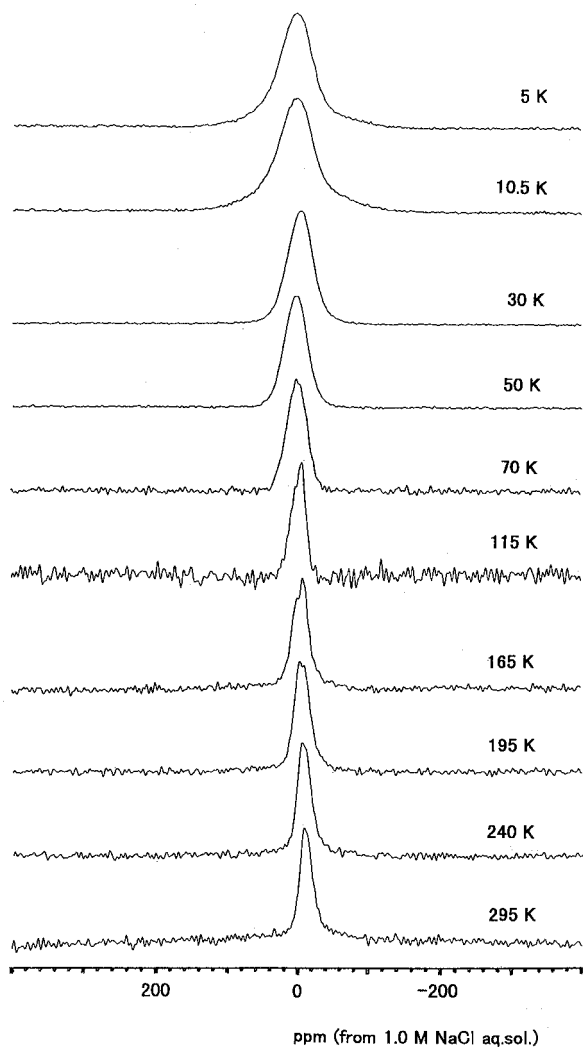


**Figure 1.** Temperature dependence of of $^{23}$Na NMR spectrum for Na(THF)$_y$C$_{60}$ single crystals.

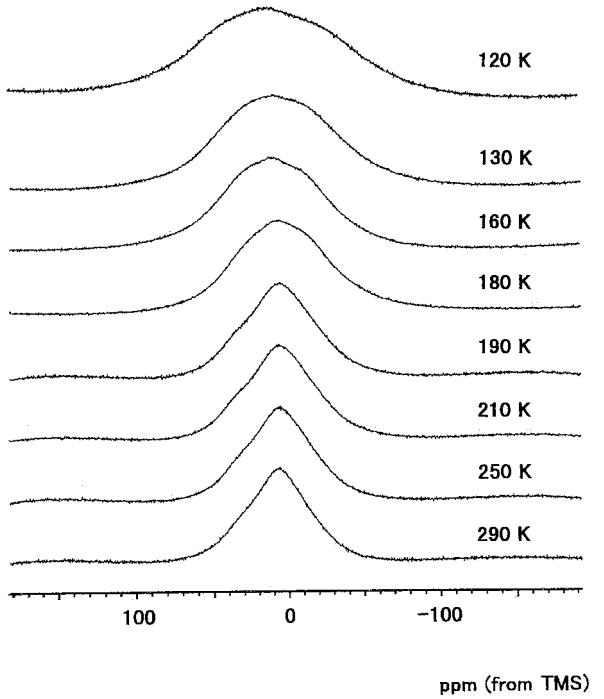


**Figure 2.** Temperature dependence of of $^1$H NMR spectrum for Na(THF)$_y$C$_{60}$ single crystals.

## IV-N-3 Magnetic Behaviors of High-Temperature Reaction Products of Cerium Metal and $C_{60}$ Solid

**MARUYAMA, Yusei[1]; SUZUKI, Kenji[1]; TAKAGI, Sigenori[1]; MOTOHASHI, Satoru[1]; OGATA, Hironori**
*([1]Housei Univ.)*

Exohedral metal doping or intercalation to $C_{60}$ solids has been known to be a very important method to modify the solid state properties of $C_{60}$ dramatically. In this study we have used Ce metal as the dopant which has the lowest melting point, 1072 K, among the lanthanide elements and has relatively low ionization potential, 5.54 eV, because it might react with $C_{60}$ solid in the liquid state. Ce metal powder and $C_{60}$ powder were mixed at the nominal stoichiometry of (1.5-1.8):1 in a quartz tube under argon atomosphere and sealed off with 50 Torr He gas after evacuation. The samples were heated in an electric furnace at 650, 700, 750, 800, 850, 900 and 1100 °C for several to 10 hours respectively. The temperature dependence of the magnetizations clearly shows the existence of ferromagnetism in these samples which could be originated in the $4f^1$ electrons of $Ce^{3+}$ ions. Figure 1 shows the *M-T* curve for 650 °C sample. The *ZFC* curve in Figure 1 is indicating the diamagnetic contribution in the temperature region of 5–15 K against the ferromagnetic uptake of the magnetization. The *M-T* curve for 1100 °C sample is shown in Figure 2. Negative magnetization is clearly observed below 10.5 K in the *ZFC* curve as shown in Figure 2, which may indicate the occurrence of superconductivity in this system.

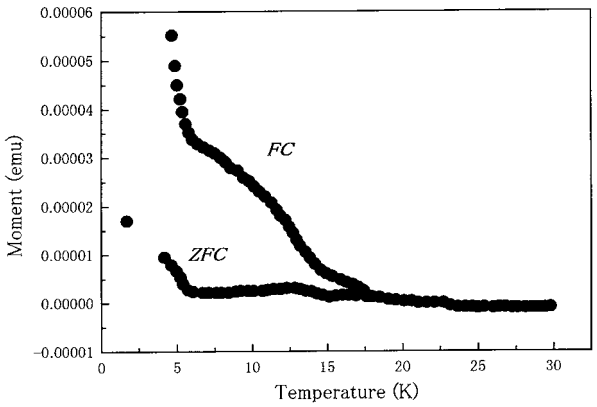


**Figure 1.** *M-T* curve of $Ce_{1.5}C_{60}$ reacted at 650 °C.

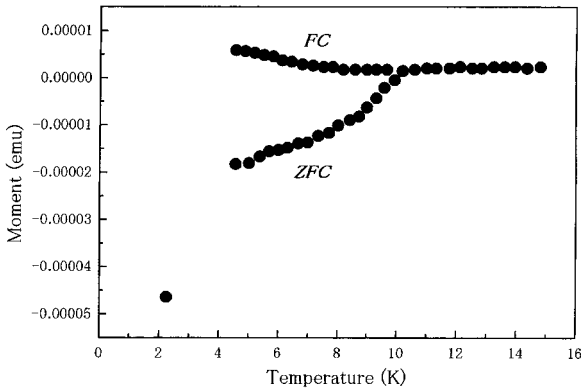


**Figure 2.** *M-T* curve $Ce_{1.5}C_{60}$ reacted at 1100 °C.

## IV-N-4 Structure and Raman Scatterings of $Cs_3C_{60}$ under High Pressure

**FUJIKI, Satoshi[1]; KUBOZONO, Yoshihiro[1]; TAKABAYASHI, Yasuhiro[1]; KASHINO, Setsuo[1]; EMURA, Shuichi[2]; FUJIWARA, Akihiko[3]; ISHII, Kenji[3]; SUEMATSU, Hiroyoshi[3]; MURAKAMI, Youichi[4]; IWASA, Yoshihiro[5]; MITANI, Tadaoki[5]; OGATA, Hironori**

*([1]Okayama Univ.; [2]Osaka Univ.; [3]Univ. Tokyo; [4]KEK-PF; [5]JAIST)*

Raman scatterings for a pressure induced superconductor $Cs_3C_{60}$ were studied in a pressure region from 1 bar to 62 kbar. The center frequency w0 for $H_g(1)$ and $H_g(2)$ Raman peaks increased by applying pressure, but it showed a saturation in high pressure region. On the other hand, the w0 for $A_g(1)$ and $A_g(2)$ modes increased straightforwardly in all pressure region. The electron-phonon coupling constant for $Cs_3C_{60}$ showed no increase at high pressures. X-ray powder diffraction patterns at 11 K under a pressure of 40 kbar showed that a superconducting phase for $Cs_3C_{60}$ was body-centered orthorhombic.